

## Exploring the Functional Performance of a Commercial High-Temperature Photopolymer Resin for Vat Photopolymerized Injection Molding Tools

Haley W. Jones\*, Andrew P. Rhodes\*, Anastasia Mullins<sup>+</sup>, Camden A. Chatham\*

\*Advanced Engineering Division, Savannah River National Laboratory, Aiken, SC USA

<sup>+</sup>Tritium Technology Division, Savannah River National Laboratory, Aiken, SC USA

### Abstract

Additive manufacturing (AM) presents a promising approach for rapid tooling, offering significant reductions in production costs and lead times compared to that of conventional mold-making processes. This work examines the fabrication of molds for injection molding through vat photopolymerization (VPP) AM, using a commercially available photopolymer resin intended for high temperature applications (High Temp V2 resin). The photorheological behavior of the resin is examined to evaluate its curing kinetics and mechanical development during polymerization, ensuring suitability for mold fabrication. The thermal and mechanical properties of the printed photopolymer resin are characterized, alongside assessments of dimensional accuracy and surface finish, which are critical factors influencing the performance and quality of injection molded parts. Additionally, specimens produced using VPP-fabricated molds are evaluated and benchmarked against those molded with traditional metal molds.

### Introduction

The traditional production of thermoplastic polymer components at scale relies heavily on formative manufacturing (FM) techniques, such as injection molding.<sup>1,2</sup> Injection molding is a high-volume FM process in which a molten polymer is injected into a mold cavity, where it cools and solidifies into the desired geometry. Injection molding using traditional metal tooling is widely used for the manufacturing of parts with high repeatability and excellent surface finish.<sup>1,2</sup> However, metal molds, commonly fabricated from aluminum or steel, are costly and energy-intensive to produce, limiting their practicality for low-volume or iterative product development.<sup>1</sup>

Recently, the production of injection molding tools using additive manufacturing (AM) has emerged as a promising area of research, enabling greater geometric freedom and faster production speeds.<sup>1</sup> Studies aimed at the evaluation of injection molding tools fabricated by AM have explored metal AM techniques, such as powder bed fusion (PBF),<sup>3</sup> and polymer AM techniques, such as materials extrusion (MEX),<sup>4</sup> material jetting (MJT),<sup>5</sup> and vat photopolymerization (VPP).<sup>6</sup> Among these AM techniques, VPP is well-known to fabricate high-resolution parts with smooth surface finishes and excellent dimensional accuracy, making VPP an compelling candidate for injection molding tools.<sup>7,8</sup>

VPP AM selectively photopolymerizes a liquid photocurable resin using ultraviolet (UV) or visible light in discrete layers, where a computer-aided design (CAD) model defines the geometry of each cross-sectional layer.<sup>7,9</sup> Recent advances in high-performance resins have made VPP increasingly viable for functional tooling applications.<sup>7,9</sup> However, the brittle nature of photopolymers, especially acrylate-based photopolymers, and their limited thermal conductivity

presents challenges regarding the longevity and mold fidelity under cyclic thermal and mechanical loads.<sup>8,10</sup> Nonetheless, VPP-fabricated molds offer a practical alternative to low-volume production and early-stage mold development, enabling rapid design iteration and performance assessment prior to investing in costly metal tooling.

This work explores the use of a commercial off-the-shelf (COTS) photocurable resin intended for high-temperature applications (High Temp V2 resin, FormLabs Inc.) in the fabrication of injection molding tools via VPP AM. Prior to mold fabrication, the rheological behavior of the resin during photopolymerization was analyzed. Additionally, the thermal properties of VPP-printed specimens were evaluated alongside the mechanical properties of tensile specimens printed in different orientations and in the green and post-cured state. An ASTM D638 type IV tensile bar mold was fabricated via VPP AM using the High Temp V2 resin and the dimensional accuracy and surface finish of the mold were examined. As an initial assessment of feasibility, a poly(lactic acid) specimen was injection molded using the VPP-fabricated tensile bar mold and compared to a specimen injection molded with a traditional metal mold.

## **Materials and Methods**

### **Materials**

The photocurable resin intended for high-temperature applications (High Temp V2 resin; FormLabs Inc.) and isopropyl alcohol (IPA) (99%, Sigma Aldrich) was used as received. Poly(lactic acid) (PLA) pellets (Ingeo Biopolymer, Grade: 4043D; NatureWorks, LLC.) for injection molding were dried in an oven set at 60°C prior to injection molding.

### **Specimen and Mold Fabrication**

Specimens and molds were designed in three-dimensional (3D) computer-aided design (CAD) software (Creo, PTC Inc.) and printed out of High Temp V2 resin using a commercial VPP system equipped with a 385 nm ultraviolet (UV) light source (Asiga Max UV, Asiga). Asiga Composer software was used to control the print parameters and slice the specimen and mold .stl files. The resin vat temperature was set at 30°C during printing. One burn-in layer with a light intensity and exposure time of 5.00 mW/cm<sup>2</sup> and 14.13 s, respectively, was used to ensure adhesion to the build plate. Subsequently, the same light intensity and shorter exposure time of 10.22 s was used to cure each additional layer. For the separation of the build plate from the bottom of the vat after each layer was printed, a velocity of 2.48 mm/s, distance of 10 mm, and pressure limit of 300 g/cm<sup>2</sup> was used. For the approach of the build plate to the resin vat after separation, a velocity of 4.30 mm/s and pressure limit of 100 g/cm<sup>2</sup> was used. For the burn-in layer, a wait time of 2 s after exposure, 5 s after separation, and 0 s after approach was used. For all subsequent layers, a wait time of 0.1 s after separation and 0 s after separation and approach was used. No supports were used in the printing of any specimen or mold.

After printing, all specimens and molds were washed with IPA and dried. All printed specimens and molds were post-cured according to manufacturer recommendations to achieve the maximum thermal and mechanical performance. All specimens and molds were rinsed with IPA and post-cured in two treatments per manufacturer (FormLabs Inc.) recommendations to achieve

the greatest thermal and mechanical properties. The first treatment ( $C_1$ ) occurred in a Form Cure (FormLabs Inc.) set at 80°C for 120 min and the second treatment ( $C_2$ ) occurred in an oven set at 160°C for 180 min.

## Injection Molding

A benchtop injection molding machine (Proto-Ject, Manning Innovations) was used to melt PLA pellets at temperatures between 200 – 240°C and mold PLA parts at injection pressures between 40 – 60 psi. VPP-printed molds were placed within a 5 x 2.5 x 1 in metal frame and clamped below the nozzle of the injection molding machine. Due to the print limitations of the Asiga Max UV printer (build volume: 4.69 x 2.64 x 2.95 in), VPP-printed mold halves of 4.63 in length were fabricated and 2 x 0.2 x 0.5 in VPP-printed inserts were fabricated to place on either side of the VPP-printed mold to keep the mold centered within the metal frame. Prior to injection molding, the face of each half of the VPP-printed mold were flattened with a CNC milling machine and alignment pins were placed at the diagonals in each half of the mold. VPP-printed molds were sprayed with Dry Film Mold Release Spray (Stoner) prior to use.

## Characterization

*Optical Spectroscopy.* An Ocean Insight solarization resistant optical fiber (QP400-2-SR) coupled to an Ocean Insight Ocean HDX miniature spectrometer was used to collect the emission spectra of the Asiga Max UV light source.

*UV/Vis Spectroscopy.* A Perkin Elmer Lambda 850 spectrometer was used to collect the absorption spectrum of the photocurable resin. A standard 10 mm pathlength quartz cuvette was utilized for all measurements.

*Fourier Transform Infrared-Attenuated Total Reflection Spectroscopy (FTIR-ATR).* A Bruker ALPHA II compact FTIR spectrometer equipped with a diamond ATR crystal (Bruker Platinum ATR QuickSnap™ Sampling Module) was used to collect FTIR-ATR spectra. All spectra were recorded by averaging 32 scans at a spectral resolution of 2  $\text{cm}^{-1}$ .

*Photorheology.* An Anton Paar MCR302e rheometer coupled with an Omnicure S2000 UV source was used to collect photorheological measurements. The Omnicure S2000 UV source was equipped with a 200 W mercury arc lamp and a 320 – 500 nm filter. A 20 mm disposable aluminum upper plate and quartz bottom plate were used for all measurements. Experiments were conducted in the linear viscoelastic region of the uncured material at 1% oscillatory strain, 10 Hz oscillation frequency, and with a gap of 100  $\mu\text{m}$ .

*Thermogravimetric Analysis (TGA).* A Mettler Toledo TGA 2 was used monitor the weight loss of the printed resin specimens with increasing temperature. TGA specimens (ca. 4 mm diameter, 2 mm height cylinders) were printed using the Asiga Max UV printer. All samples were run in 80  $\mu\text{L}$  alumina crucibles at a heating rate of 20°C/min in a nitrogen or air atmosphere.

*Differential Scanning Calorimetry (DSC).* A Mettler Toledo DSC 3+ was used to evaluate the thermal transitions of the VPP-fabricated specimens. DSC specimens (ca. 4 mm diameter, 0.5

mm height cylinders) were printed using the Asiga Max UV printer. Samples were run in 40  $\mu$ L aluminum pans at a heating/cooling rate of 10°C/min in a nitrogen atmosphere. All samples were run from 0 – 250°C on the first heating cycle to determine if any additional curing occurred after printing and erase any thermal memory from the specimens. A second heating cycling from -20 – 250°C was used to determine the glass transition temperature ( $T_g$ ) of the specimens.

*Tensile Testing.* An MTS Criterion Model 43 electromechanical universal test system equipped with a 10 kN load cell was used to perform tensile tests according to ASTM D638. Type V specimens were fabricated using the Asiga Max UV printer in different build orientations. To assess the effect of the print orientation on the mechanical properties of the resin, specimens ( $\geq n=5$  each group) were printed horizontally with the layers deposited along the thickness of the specimen (X-orientation), horizontally with the layers deposited along the width of the specimen (Y-orientation), and vertically, with the layers deposited along the length of the specimen (Z-orientation). The specimens printed in different build orientations were all exposed to both post-cure treatments ( $C_2$ ). To assess the evolution of mechanical properties in the green and post-cured ( $C_1$ , and  $C_2$ ) state, all specimens ( $\geq n=5$  each group) were printed vertically with the layers deposited along the length of the specimen (Z-orientation). For all tensile tests, a gauge length of 7.62 mm and a test speed of 1 mm/min was used.

*Optical Microscopy.* A Keyence VR-6200 3D optical profilometer was used to obtain optical images (12x magnification) and measure the dimensional accuracy and surface finish of the VPP-fabricated mold and injected tensile bar specimens.

## Results and Discussion

In the efforts towards functional injection molding tools via vat photopolymerization (VPP) additive manufacturing (AM) for low-volume production and iterative mold design optimization, a commercial off-the-shelf (COTS) photopolymer resin intended for high-temperature applications (High Temp V2 resin) was investigated. Initially, the optical absorbance of the photocurable resin and spectral output of the VPP AM system's ultraviolet (UV) light source was collected to ensure good spectral overlap such that the resin could be photopolymerized to fabricate a solid three-dimensional (3D) object. **Figure 1a** presents the absorbance spectrum of High Temp V2 resin in isopropyl alcohol (IPA), where three peaks at 365 nm, 382 nm, and 404 nm are observed. The emission spectrum of the VPP AM system (Asiga Max UV printer) is presented in **Figure 1b**, where a single sharp peak at 385 nm is observed, confirming adequate spectral overlap at the maximum absorption of the resin for VPP AM.

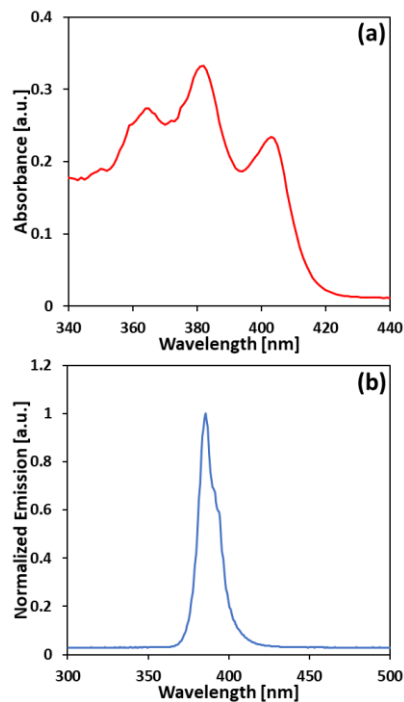


**Figure 1.** (a) Absorption spectrum of 1 % w/v High Temp V2 resin in isopropyl alcohol. (b) Emission spectrum of the Asiga Max UV light source.

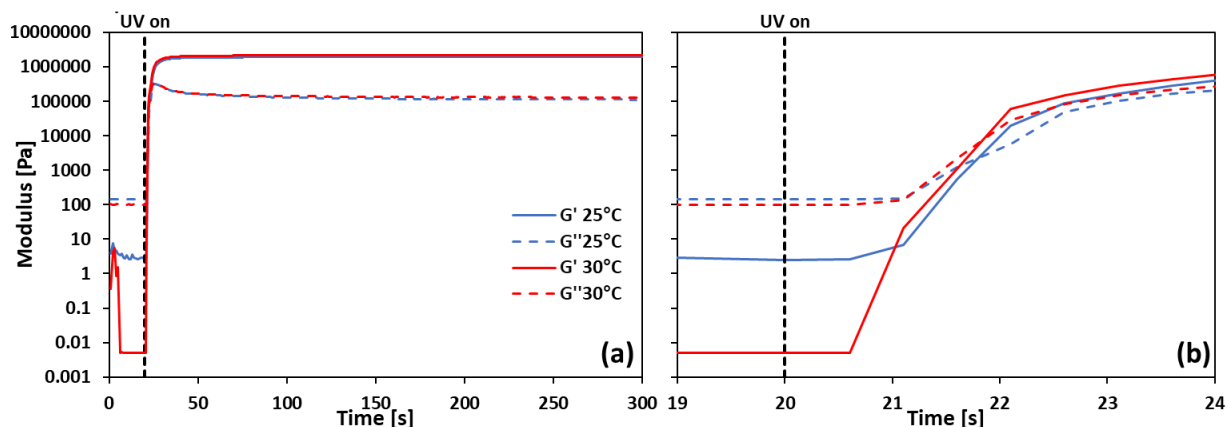


**Figure 2.** (a) Evolution of the storage ( $G'$ ; solid lines) and loss ( $G''$ ; dashed lines) modulus of High Temp V2 resin upon exposure to UV light ( $5 \text{ mW/cm}^2$ ) at  $25^\circ\text{C}$  (blue lines) and  $30^\circ\text{C}$  (red lines). (a) is presented on a constrained timescale in (b) such that the time to modulus crossover after UV exposure can be observed. UV exposure occurred at 20 s with a 100 ms delay and remained constant for the remainder of the data acquisition.

The Asiga Max UV VPP system is equipped with a heater such that the photocurable resin could be warmed to  $30^\circ\text{C}$  during printing (i.e., the manufacturer recommended print temperature), decreasing the viscosity of the resin and allowing for faster print speeds. The photorheological behavior of the resin at  $30^\circ\text{C}$  with a UV irradiance of  $5 \text{ mW/cm}^2$  is presented in **Figure 2**, where the time to gelation (modulus crossover) was ca. 1.52 s. The time to reach 90% of the maximum storage modulus was 18.5 s, while the time to reach the maximum storage modulus (ca. 2.22 MPa) was 258 s. Comparatively, when the temperature of the resin was  $25^\circ\text{C}$  with a UV irradiance of  $5 \text{ mW/cm}^2$ , the time to gelation was ca. 1.53 s and the time to reach 90% and 100% of the maximum storage modulus (ca. 1.95 MPa) was 16.5 s and 290 s, respectively. Notably, the maximum storage modulus of the cured resin when the temperature was  $30^\circ\text{C}$  was 14% greater than when the temperature was  $25^\circ\text{C}$ . Additionally, a significant decrease (ca. 28%) in the measured complex viscosity of the resin at  $30^\circ\text{C}$  (1628 cP at 1 Hz) compared to that at  $25^\circ\text{C}$  (2274 cP at 1 Hz) was detected, indicating a reduced viscoelastic resistance at the manufacturer recommended printing

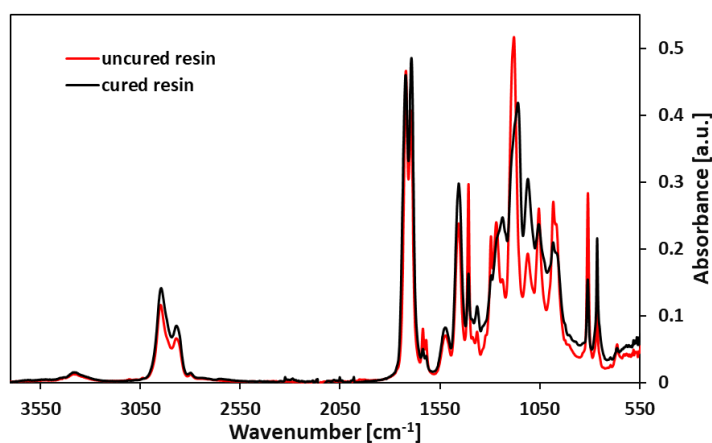


**Figure 3.** FTIR-ATR spectra of uncured and cured FormLabs High Temp V2 resin.

temperature. **Figure 3** presents the Fourier transform infrared-attenuated total reflection (FTIR-ATR) spectra of the uncured resin and the  $100 \mu\text{m}$  thin film cured on the rheometer at  $30^\circ\text{C}$ . The FTIR spectra of the cured resin exhibits decreased peak intensities attributed to  $\text{C}=\text{C}$  at  $1635 \text{ cm}^{-1}$  and  $=\text{CH}_2$  at  $1407 \text{ cm}^{-1}$  compared to that of the uncured resin, attributed to the polymerization of the resin monomers upon exposure to UV light.

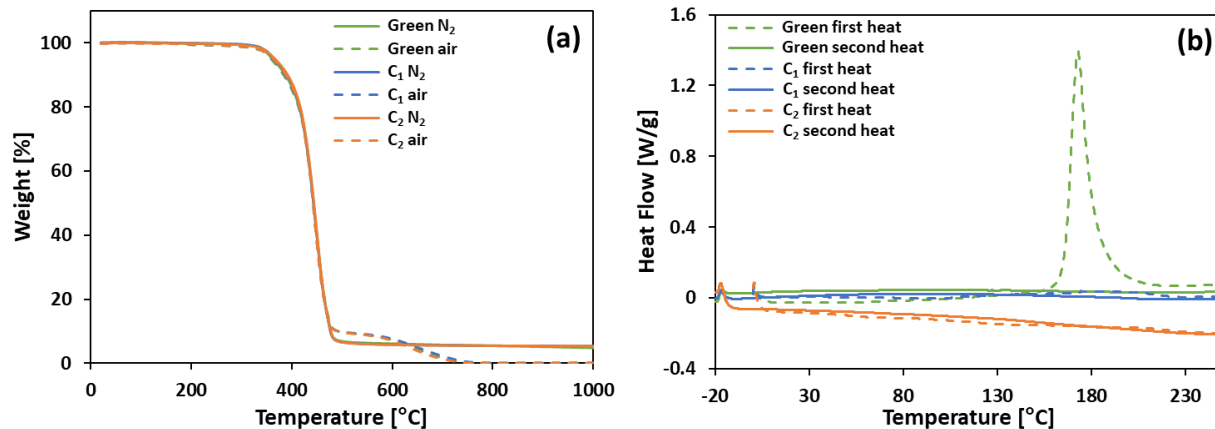


**Figure 4.** (a) TGA curves of green and post-cured (C<sub>1</sub> and C<sub>2</sub>) High Temp V2 resin specimens fabricated by VPP in nitrogen (N<sub>2</sub>) and air atmospheres. (b) DSC curves of green and post-cured (C<sub>1</sub> and C<sub>2</sub>) High Temp V2 resin specimens fabricated by VPP.

To investigate the applicability of the printed resin in high-temperature applications, such as injection molding, the thermal properties of the resin were investigated. To this end, specimens for thermogravimetric analysis (TGA) and differential scanning calorimetry (DSC) were fabricated using the Asiga Max UV VPP AM system. Once fabricated, the green specimens were rinsed with IPA to remove any uncured resin and dried. After drying, the specimens underwent up to two manufacturer recommended post-cure treatments (C<sub>1</sub> and C<sub>2</sub>; cf. Materials and Methods) to achieve the greatest thermal and mechanical properties. As shown in **Figure 4a**, the green and post-cured specimens exhibit similar thermal stability in air and nitrogen atmospheres, respectively. In a nitrogen atmosphere, a 2% weight loss was observed at 343°C, 345°C, and 345°C for the green, C<sub>1</sub>, and C<sub>2</sub> specimens, respectively. By 1000°C, a ca. 95% weight loss was observed for all specimens. In an air atmosphere, a 2% weight loss was observed at 334°C, 334°C, and 335°C for the green, C<sub>1</sub>, and C<sub>2</sub> specimens, respectively. By 1000°C, a ca. 99.9% weight loss was observed for all specimens. Measurements by DSC are presented in **Figure 4b**, where additional

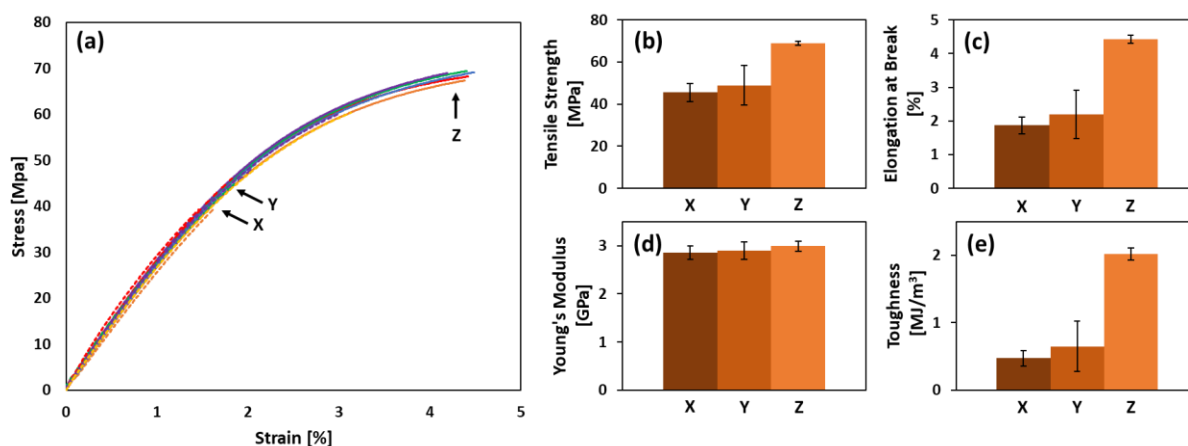


**Figure 5.** (a) Stress-strain curves of High Temp V2 type V tensile bar specimens fabricated in the X-, Y-, and Z-orientation ( $\geq n=5$  all groups). Average (b) tensile strength, (c) elongation at break, (d) Young's modulus, and (e) toughness of the High Temp V2 type V tensile bar specimens fabricated in the X-, Y-, and Z-orientation ( $\geq n=5$  all groups).

curing is observed in the first heat of the green specimen with an onset at ca. 150°C and a peak at 173°C. The post-cured specimens did not exhibit any additional curing in the first heat. A discernable glass transition temperature ( $T_g$ ) was not observed in the second heat of the green or post-cured specimens, indicating a high degree of crosslinking.

The tensile properties of the fully post-cured ( $C_2$ ) High Temp V2 resin when printed in different build orientations (X-, Y-, and Z-orientation) are presented in **Figure 5**. The stress-strain curves of the specimens in different build orientations are shown in **Figure 5a**, where all specimens demonstrate a brittle response, characterized by a steep linear elastic region followed by sudden fracture with minimum plastic strain. Interestingly, the highest tensile strength of  $68.9 \pm 1.0$  MPa was observed for the specimens fabricated in the Z-orientation, when the layers were perpendicular to the loading direction (cf. **Figure 5b**). When the layers were parallel to the loading direction in the specimens fabricated in the X- and Y-orientation, a tensile strength of  $45.5 \pm 4.4$  MPa and  $49.0 \pm 9.5$  MPa was observed, respectively. The specimens fabricated in the Z-orientation exhibited the greatest elongation at break of  $4.4 \pm 0.1\%$  compared to that of the X- and Y-orientation specimens, which were  $1.9 \pm 0.2\%$  and  $2.2 \pm 0.7\%$ , respectively (cf. **Figure 5c**). Young's modulus of the specimens was determined by the slope of the linear region of the stress-strain curves presented in **Figure 5a**. As shown in **Figure 5d**, a similar modulus of  $2.86 \pm 0.14$  GPa,  $2.90 \pm 0.18$  GPa, and  $3.00 \pm 0.10$  GPa was observed for the specimens fabricated in the X-, Y-, and Z-orientation, respectively. Lastly, the toughness of the specimens was determined by integrating the area under the stress-strain curves presented in **Figure 5a**. The specimens fabricated in the Z-orientation exhibited the greatest toughness of  $2.0 \pm 0.1$  MJ/m<sup>3</sup> while the X- and Y-orientation specimens exhibited a toughness of  $0.5 \pm 0.1$  MJ/m<sup>3</sup> and  $0.7 \pm 0.4$  MJ/m<sup>3</sup>, respectively. The observed increase in tensile strength, elongation at break, and toughness of the specimens fabricated in the Z-orientation may be attributed to the reduced curing nonuniformities in the XY plane due to the smaller cross-sectional area of each layer. Nonuniform curing in the XY plane can impart in-layer defects or residual stress in the final part, leading to premature failure. This phenomenon of increased tensile properties in VPP Z-orientation builds has been demonstrated in the literature.<sup>11</sup>

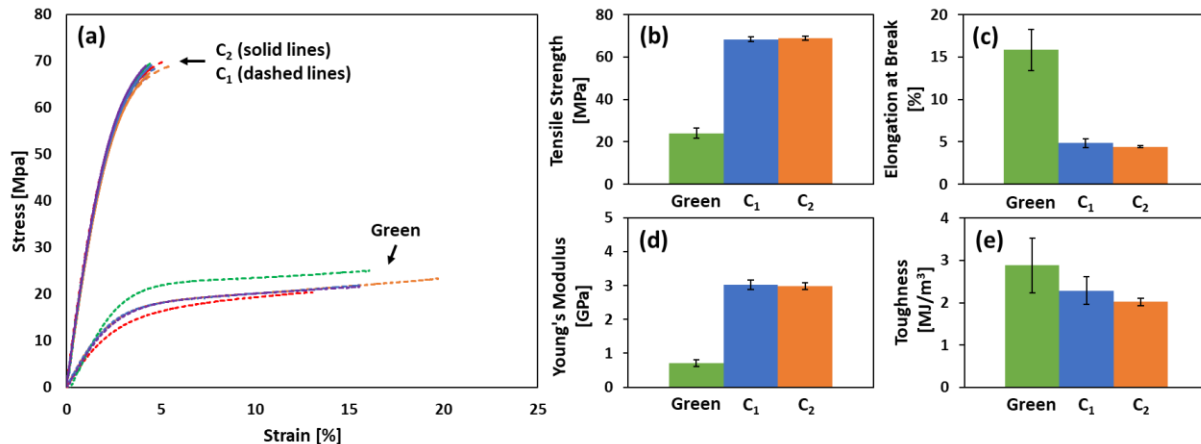


**Figure 6.** (a) Stress-strain curves of green and post-cured ( $C_1$  and  $C_2$ ) High Temp V2 type V tensile bar specimens ( $\geq n=5$  each group) fabricated in the Z-orientation. Average (b) tensile strength, (c) elongation at break, (d) Young's modulus, and (e) toughness of green and post-cured ( $C_1$  and  $C_2$ ) High Temp V2 type V tensile bar specimens ( $\geq n=5$  each group) fabricated in the Z-orientation.

	Green <sup>12</sup>	Green [Z]	C <sub>1</sub> <sup>12</sup>	C <sub>1</sub> [Z]	C <sub>2</sub> <sup>12</sup>	C <sub>2</sub> [X]	C <sub>2</sub> [Y]	C <sub>2</sub> [Z]
Tensile Strength [MPa]	20.9	24.1 ± 2.4	58.3	68.4 ± 1.1	51.1	45.5 ± 4.4	49.0 ± 9.5	68.9 ± 1.0
Elongation at Break [%]	14	15.9 ± 2.4	3.3	4.8 ± 0.5	2.4	1.9 ± 0.2	2.2 ± 0.7	4.4 ± 0.1
Modulus [GPa]	0.75	0.72 ± 0.10	2.75	3.02 ± 0.14	2.90	2.86 ± 0.14	2.90 ± 0.18	3.00 ± 0.10

**Table 1.** Manufacturer reported tensile properties<sup>12</sup> (red) compared to the measured tensile properties (black) of green (Z-direction), C<sub>1</sub> (Z-direction), and C<sub>2</sub> (X-, Y-, and Z-direction) specimens.

The tensile properties of green and post-cured High Temp V2 type V tensile bar specimens fabricated in the Z-orientation are presented in **Figure 6**. The stress-strain curves of the green and post-cured specimens are shown in **Figure 6a**, where the green specimens exhibit behavior characteristic of a ductile material, with a substantial plastic deformation prior to failure. In contrast, the C<sub>1</sub> and C<sub>2</sub> post-cured specimens display a more brittle response. This shift in mechanical behavior is attributed to the increased crosslinking density and rigidity after post-curing. Not surprisingly, the green specimens exhibited a significantly lower tensile strength of  $24.1 \pm 2.4$  MPa compared to the post-cured specimens (cf. **Figure 6b**). C<sub>1</sub> and C<sub>2</sub> post-cured specimens exhibited similar tensile strengths of  $68.4 \pm 1.1$  MPa and  $68.9 \pm 1.0$  MPa, respectively. A  $15.9 \pm 2.4\%$  elongation at break was observed for the green specimens while a  $4.8 \pm 0.5\%$  and  $4.4 \pm 0.1\%$  elongation at break was observed for the C<sub>1</sub> and C<sub>2</sub> post-cured specimens, respectively (cf. **Figure 6c**). The Young's modulus of the green specimens was determined to be  $0.72 \pm 0.10$  GPa, while that of the C<sub>1</sub> and C<sub>2</sub> specimens was  $3.02 \pm 0.14$  GPa and  $3.00 \pm 0.10$  GPa, respectively (cf. **Figure 6d**). The green specimens displayed the highest toughness of  $2.9 \pm 0.6$  MJ/m<sup>3</sup> followed by the C<sub>1</sub> specimens with a toughness of  $2.3 \pm 0.3$  MJ/m<sup>3</sup> and the C<sub>2</sub> specimens with a toughness of  $2.0 \pm 0.1$  MJ/m<sup>3</sup> (cf. **Figure 6e**). While a significant increase in mechanical properties was observed after post-curing, the mechanical properties of specimens that underwent the first post-cure treatment (C<sub>1</sub>) and the second post-cure treatment (C<sub>2</sub>) were comparable.

**Table 1** presents the tensile properties of

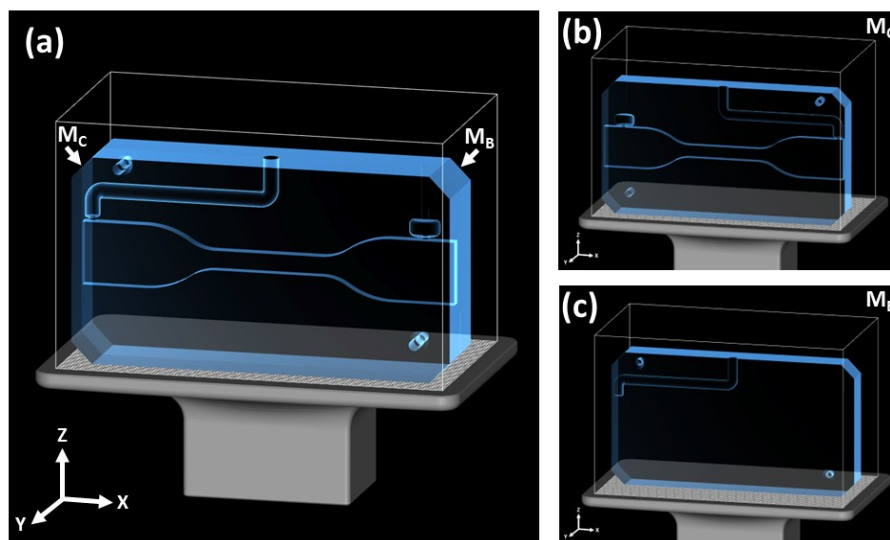


**Figure 7.** X-ray mode images of the two halves of the ASTM D638 type IV tensile bar mold (M<sub>C</sub> and M<sub>B</sub>) (a) aligned and (b,c) separated in the Asiga Composer software. The molds were fabricated vertically in the Z-orientation, as shown, in the same build without mating. The print time was ca. 2.5 hours.

the green and post-cured ( $C_1$  and  $C_2$ ) specimens reported by the manufacturer<sup>12</sup> compared to the measured tensile properties of green and post-cured ( $C_1$  and  $C_2$ ) specimens printed in the Z-direction and the post-cured ( $C_2$ ) specimens printed in the X- and Y-direction. It is important to note that the tensile properties reported by the manufacturer were obtained from specimens printed on a Form 2 (FormLabs Inc.) printer (i.e., a stereolithography-based printer equipped with a 405 nm laser) in an unspecified direction. The measured tensile properties of the green specimens printed in the Z-direction were in good agreement with the manufacturer reported tensile properties. However, the tensile properties of the post-cured specimens ( $C_1$  and  $C_2$ ) printed in the Z-direction were notably higher than that of the manufacturer reported properties. The manufacturer reported tensile properties of the  $C_2$  specimens most closely matched those of the  $C_2$  specimens printed in the X- and Y-direction. These differences in tensile properties can be attributed to differences in print orientation and settings as well as cure technology and wavelength (i.e., a 405 nm stereolithography-based printer vs a 385 nm digital light processing-based printer).

To evaluate the applicability of FormLabs High Temp V2 resin in injection molding applications, an ASTM D638 Type IV tensile bar specimen mold was designed using a 3D computer-aided design (CAD) software (Creo) to produce a Type IV tensile bar upon the injection of molten polymer as shown in **Figure 7**. The tensile bar mold was design such that only one half of the mold contained the tensile bar specimen cavity ( $M_C$ ; cf. **Figure 7b**) and the other half of the mold was “blank” ( $M_B$ ; cf. **Figure 7c**). A 2.35 mm diameter open semi-circle channel running from the top center of each half of the mold was design such that when the molds were mated, a 4.7 mm channel lead the molten polymer into the top of one side of the tensile bar cavity. A vent pocket (9.5 diameter, 4.8 mm height open semi-circle) and a 16.5 mm length open rectangular channel (2.3 mm x 0.13 mm) on the tensile bar half of the mold was positioned at the top of the opposite side of the tensile bar cavity to allow for air to escape from the cavity during injection. Additionally, two 3.25 mm diameter alignment pin holes were added at corners diagonally from each other on each half of the mold to accommodate guide pins, ensuring proper mating and alignment of the mold. Photographs of both halves of the VPP-fabricated injection mold ( $M_C$  and  $M_B$ ) in their green and post-cured states are presented in **Figure 8**. **Table 2** presents the dimensions of the as-designed tensile bar cavity in  $M_C$  compared to the

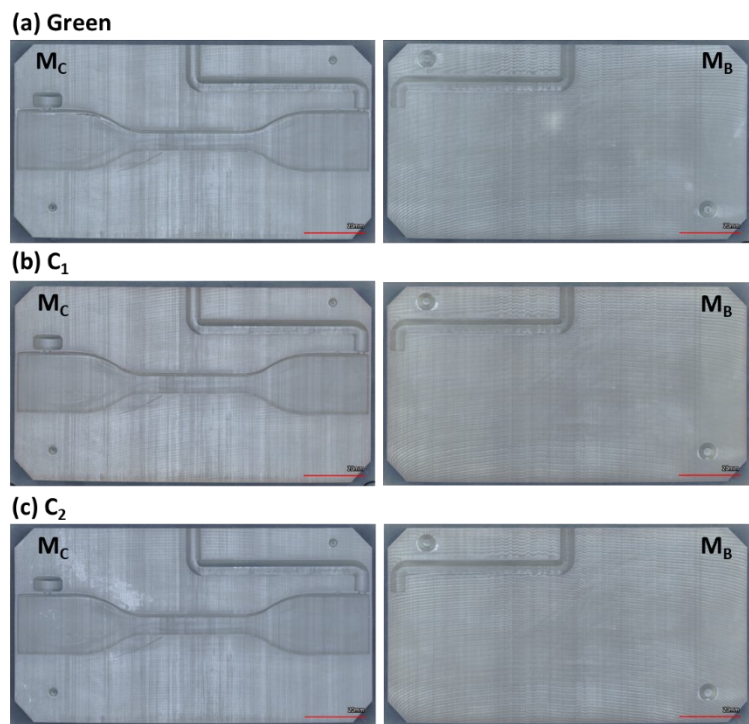
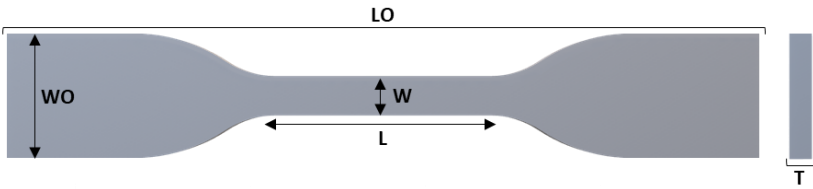


**Figure 8.** Images of the tensile bar cavity ( $M_C$ ) and “blank” ( $M_B$ ) half of the VPP-fabricated injection mold in its (a) green state, (b) after the first post-cure treatment ( $C_1$ ), and (c) after the second post-cure treatment ( $C_2$ ).

measured dimensions of the cavity in the VPP-fabricated green and post-cured mold. The cavity dimensions in the X-direction showed good dimensional fidelity (within  $\pm 0.5\%$ ), while dimensions in the Y- and Z-direction showed a ca. 1.5% and 3% shrinkage, respectively. Throughout the post-processing treatments of the VPP-fabricated mold, the dimensions and relatively smooth surface finish, especially compared to other AM techniques,<sup>13</sup> of the tensile bar cavity remained consistent (cf. **Table 2**).



	W [mm]	L [mm]	WO [mm]	LO [mm]	T [mm]	Sa [ $\mu\text{m}$ ]
<b>As-Designed</b>	6.0	34.0	19.45	115.0	3.7	N/A
<b>Green Mold</b>	$5.5 \pm 0.2$	$34.2 \pm 0.3$	$18.8 \pm 0.6$	$114.9 \pm 0.4$	$3.7 \pm 0.1$	$1.9 \pm 0.7$
<b>C<sub>1</sub> Mold</b>	$5.6 \pm 0.1$	$34.2 \pm 0.1$	$19.6 \pm 0.5$	$115.1 \pm 0.1$	$3.6 \pm 0.1$	$2.0 \pm 0.9$
<b>C<sub>2</sub> Mold</b>	$5.8 \pm 0.1$	$34.2 \pm 0.2$	$19.4 \pm 0.3$	$115.6 \pm 0.5$	$3.6 \pm 0.1$	$1.9 \pm 0.7$
<b>Injected Tensile Bar</b>	$5.7 \pm 0.2$	$34.6 \pm 0.1$	$19.3 \pm 0.2$	$114.6 \pm 0.2$	$3.7 \pm 0.1$	$8.8 \pm 2.0$

**Table 2.** Measured (n=3) dimensions (W, L, WO, LO, and T) and average surface roughness (Sa) of the tensile bar cavity in the green and post-cured (C<sub>1</sub> and C<sub>2</sub>) mold compared to the as-designed dimensions and measured dimensions of the injection molded PLA tensile bar using the VPP-fabricated mold.

Finally, the VPP-printed mold was used to produce an injection molded poly(lactic acid) (PLA) tensile bar specimen. The two halves of the VPP-fabricated tensile bar mold were aligned using guide pins and placed within a metal frame with a 4.7 mm diameter hole in the top center to allow for molten polymer injection into the mold. The VPP-fabricated mold was heated with a mold heater set at 80°C during injection molding and was able to withstand melt temperatures of up to 210°C and injection pressures of up to 3300 psi. **Figure 9** presents a photograph of the injection molded PLA tensile bar specimen produced using the VPP-fabricated mold compared to a PLA tensile bar specimen produced using a traditional metal mold. While the mold cavity geometry was replicated by the injected PLA with high fidelity ( $\pm 1\%$ ), trapped air was present within the tensile bar specimen, suggesting a need for optimized injection parameters and mold design with additional air channels. Moreover, the average surface roughness

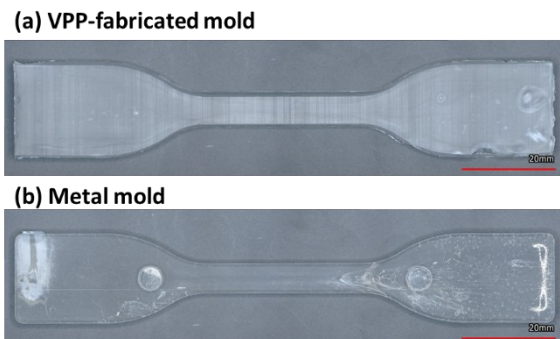


**Figure 9.** Images of injection molded tensile specimens produced using the (a) mold fabricated by VPP and (b) a metal mold.

of the specimen produced using the VPP-fabricated mold was notably higher than that of the mold itself.

### **Conclusions**

This study demonstrates the feasibility of using vat photopolymerization (VPP) additive manufacturing (AM) to fabricate injection molding tools using a commercial off-the-shelf (COTS) photocurable resin aimed at high temperature applications. VPP-fabricated molds offer faster turnaround speeds at a much lower cost compared to traditional metal molds, presenting a practical method for rapidly producing injection molds, especially for prototyping and low-volume production. While the use of the COTS resin investigated in this work may be limited due to its brittle nature, advancements in resin formulation continue to extend the feasible use window of VPP-printed tooling. Additionally, innovative mold designs tailored specifically for AM hold potential to further enhance the performance and reliability of VPP-fabricated injection molding tools.

### **Acknowledgements**

The authors thank Mark Hudson and James (“Jimmy”) Asbell for their help in mold conceptualization and design in Creo. This work was produced by Battelle Savannah River Alliance, LLC under contract number 89303321CEM000080 with the U.S. Department of Energy (DOE). Publisher acknowledges the U.S. Government license to provide public access under the DOE Public Access Plan (<http://energy.gov/downloads/doe-public-access-plan>). Direct funding was provided through the U.S. DOE’s National Nuclear Security Administration (NNSA) Additive Coordination Team (ACT).

### **References**

- 1 Dizon, J. R. C., Valino, A. D., Souza, L. R., Espera Jr, A. H., Chen, Q. & Advincula, R. C. Three-dimensional-printed molds and materials for injection molding and rapid tooling applications. *MRS Communications* **9**, 1267-1283 (2019).
- 2 Chen, Z. & Turng, L. S. A review of current developments in process and quality control for injection molding. *Advances in Polymer Technology: Journal of the Polymer Processing Institute* **24**, 165-182 (2005).
- 3 Cunha, Â., Marques, A., Silva, M. R., Bartolomeu, F., Silva, F. S., Gasik, M., Trindade, B. & Carvalho, Ó. Laser powder bed fusion of the steels used in the plastic injection mould industry: a review of the influence of processing parameters on the final properties. *The International Journal of Advanced Manufacturing Technology* **121**, 4255-4287 (2022).
- 4 Gohn, A. M., Brown, D., Mendis, G., Forster, S., Rudd, N. & Giles, M. Mold inserts for injection molding prototype applications fabricated via material extrusion additive manufacturing. *Additive Manufacturing* **51**, 102595 (2022).
- 5 Simpson, P., Zakula, A. D., Nelson, J., Dworshak, J. K., Johnson, E. M. & Ulven, C. A. Injection molding with an additive manufactured tool. *Polymer Engineering & Science* **59**, 1911-1918 (2019).
- 6 Jian, X., Gong, K., Moritz, V., Portela, A., Lu, Y., Du, W. & Major, I. Comparative evaluation of vat photopolymerization and steel tool molds on the performance of injection

- molded and overmolded tensile specimens. *Polymer Engineering & Science* **64**, 5750-5760 (2024).
- 7 Appuhamillage, G. A., Chartrain, N., Meenakshisundaram, V., Feller, K. D., Williams, C. B. & Long, T. E. 110th Anniversary: Vat photopolymerization-based additive manufacturing: current trends and future directions in materials design. *Industrial & Engineering Chemistry Research* **58**, 15109-15118 (2019).
- 8 Becerra-Borges, Y. E., Cazón-Martín, A., Rodríguez-Ferradas, M. I., Morer-Camo, P., Etxaniz-Sein, U., Manchado, J. C. & Candal, M. V. Transforming plastic injection molding with additive manufacturing: a novel systematic review of innovative approaches to insert production. *Rapid Prototyping Journal* **31**, 200-217 (2025).
- 9 Zhang, F., Zhu, L., Li, Z., Wang, S., Shi, J., Tang, W., Li, N. & Yang, J. The recent development of vat photopolymerization: A review. *Additive Manufacturing* **48**, 102423 (2021).
- 10 Ligon-Auer, S. C., Schwentenwein, M., Gorsche, C., Stampfl, J. & Liska, R. Toughening of photo-curable polymer networks: a review. *Polymer Chemistry* **7**, 257-286 (2016).
- 11 Cheadle, A. M., Maier, E., Palin, W. M., Tomson, P. L., Poologasundarampillai, G. & Hadis, M. A. The impact of modifying 3D printing parameters on mechanical strength and physical properties in vat photopolymerisation. *Scientific Reports* **15**, 12592 (2025).
- 12 FormLabs Material Properties – HIGH TEMP: Photopolymer Resin for Form 2 3D Printers. *FormLabs, Inc. Rev. 02*, 12/05/2018
- 13 Golhin, A. P., Tonello, R., Frisvad, J. R., Grammatikos, S. & Strandlie, A. Surface roughness of as-printed polymers: A comprehensive review. *The International Journal of Advanced Manufacturing Technology* **127**, 987-1043 (2023).